This manuscript is a preprint and is published in the **Journal of South American Earth Sciences** (Special Issue "*Brazilian offshore magmatism and Atlantic evolution*").

Please feel free to contact us with any comments or feedback on our study.

Please cite this work as:

https://doi.org/10.1016/j.jsames.2023.104314

Post-salt magmatism in the Campos Basin, offshore SE Brazil: style, distribution, and relationship to salt tectonics

Francyne Bochi do Amarante[1,#]

[1] Instituto de Geociências, Universidade Federal do Rio Grande do Sul, Porto Alegre, 90650 001, Brazil

[#] corresponding author francyne.amarante@ufrgs.br

ORCID https://orcid.org/0000-0003-4452-8635

Christopher Aiden-Lee Jackson[2,3]

[2] Jacobs, Manchester, M15 4GU, United Kingdom

[3] Basins Research Group (BRG), Department of Earth Science and Engineering, Imperial College London, London, SW7 2BP, United Kingdom

c.jackson@imperial.ac.uk

ORCID https://orcid.org/0000-0002-8592-9032

Leonardo Muniz Pichel[4]

[4] Department of Earth Science, University of Bergen, 5007, Bergen, Norway

leonardo.m.pichel@uib.no

ORCID https://orcid.org/0000-0001-8692-3831

Abstract

Substantial magmatism occurred during the development of the marginal basins of the central and southern South Atlantic. Situated on the Brazilian side of the central segment, the Campos and Santos basin represent a transitional margin, located between the magma-rich margin in the north and the magma-poor margin in the south. In addition to magmatism associated with the initiation of continental rifting, the southeast Brazilian basins experienced three main magmatic events; one during the early post-rift (i.e., sag stage) and two during the late post-rift (i.e., passive margin stage), both occurring after deposition of a thick, late Aptian salt layer. The products of post-salt, intrusive and extrusive magmatism in the southern Campos Basin are imaged in seismic reflection data and have been directly penetrated by boreholes, yet they remain poorly understood in terms of their style, detailed geometry, and distribution. Furthermore, the temporal, spatial and possibly genetic relationships between these post-salt igneous products and salt-tectonics are largely unknown. Documenting these possible salt-magma interactions is important to understanding the tectono-stratigraphic evolution of Campos Basin and other salt-bearing passive margin basins subject to magmatic activity. We use 2D and 3D seismic reflection and borehole data from the southeastern Campos Basin, offshore Brazil to map and characterize post-salt igneous sills and volcanoes, and to understand the interaction between salt tectonics and igneous products. We identified 99 sills emplaced within uppermost Aptian-to-Maastrichtian strata, 83 emplaced above the salt and 16 intra-salt, and 15 volcanoes within Upper Cretaceous-to-lower Paleogene strata, associated with a >310 km² lava field. We also identify four, subsalt-sourced, vent-like structures, which vary in age from Paleogene to Late Cretaceous. Salt and overburden structures define a domain of extensional deformation on a base-salt basement high, and a domain of contractional deformation in the adjacent basement low. The relationship between igneous intrusions and salt tectonics is complex, i.e., in areas where they are common, sills appear to have locally restricted salt flow and the growth of large salt structures, whereas in other cases, salt structures and

Please cite as https://doi.org/10.1016/j.jsames.2023.104314

overlying faults appear to have partially acted as pathways to intruding magma, allowing it to ascend to relatively shallow depths. Extrusive igneous products exclusively developed after the main phase of salt movement. However, salt distribution influenced the location of volcanoes, given the latter developed where salt is welded or very thin. Salt flow and thickness also controlled the distribution of lava flow products, which accumulated in structural lows between large salt tectonic structures. Our work indicates a complex relationship between salt tectonics and magmatic emplacement that impact the post-rift evolution of Campos Basin.

Keywords: offshore magmatism, igneous intrusions, igneous extrusions, Cabo Frio High, South Atlantic basins, late Cretaceous.

1. Introduction

Based on the volume of magmatic products that they contain, rifted margins are classified as either magma-rich or magma-poor (e.g. Chang et al., 1992; Demercian et al., 1993; Mohriak et al., 2020). The central segment of South-Atlantic is considered magma-poor (Aslanian et al., 2009; Contreras et al., 2010; Contrucci et al., 2004; Mohriak et al., 2008). The Campos and Santos basins, which compose the southern part of the western, Brazilian side of the central segment, have recently been interpreted to represent a transitional margin, passing from magma-poor in the north, to magma-rich in the south (e.g. Zalan et al., 2009; Evain et al., 2015). This classification is, however, based primarily on the amount of rift-related magmatism, despite the fact important episodes of magmatic activity occurred during the post-rift evolution of the southeast Brazilian basins, after deposition of a thick (up to 2 km), extensive (>741,000 km^2), Aptian salt layer (Thomaz Filho, 2008). The post-rift, Late Cretaceous to Paleogene magmatic events offshore southeast Brazil are particularly well-expressed in two provinces, (1) along the Vitória-Trindade Chain, an E-trending ridge located in the Espírito Santo Basin, south of the Abrolhos Volcanic Complex; and (2) the Cabo Frio High, a structural feature that

Please cite as https://doi.org/10.1016/j.jsames.2023.104314

separates the Campos and Santos basins (Almeida, 2006; Mohriak et al., 2020). Detailing the style, timing, and distribution of igneous products in the marginal basins offshore southeastern Brazil is key to understanding the longer-term geodynamic and tectono-stratigraphic evolution of this, with our seismic-stratigraphic approach also applicable to other rifted margins.

Understanding the distribution of and controls on post-salt igneous products in marginal basins offshore southeastern Brazil also requires an understanding of their link with underlying Aptian salt and related structures, which controlled the overall basin geometry during magmatism. Previous studies indicate salt rheology can control the style and distribution of products related to crustal magmatism, with rising magma interacting chemically and physically with its host rocks (e.g. Heimdal et al., 2019; López-García et al., 2020; Li et al., 2009, Schofield et al., 2014; Fiduk et al., 2004; Magee et al., 2021). For example, Fiduk et al. (2014) interpret that rising magma preferentially intruded pre-existing salt structures and associated faults, with the latter acting as high-permeability pathways through the overwise very fine-grained, low permeability sedimentary section. Even though the South Atlantic basins contains thick, extensive salt and were subject to important post-salt magmatic events, there are only, to the best of our knowledge, two studies that address the relationship between the two (Espírito Santo Basin; Fiduk et al., 2004; Santos Basin; Magee et al., 2021).

The southeast Campos Basin, near the Cabo Frio High, contains significant subsurface evidence for post-rift magmatism. For example, sills, volcanoes, and other volcanic products (e.g. hydrothermal vents, lava flows, and dikes) have been documented with seismic reflection data (Figure 1; e.g. Oreiro et al., 2008; Alvarenga et al., 2016; Correia et al., 2019; Mohriak et al., 2021). However, only one of these studies (Correia et al., 2019) conducted detailed mapping of the geometry and distribution of the intrusive elements of these igneous products (primarily sills), but none have addressed the spatial relationship between post-rift (post-salt) igneous products and salt tectonics in the Campos Basin.

Please cite as https://doi.org/10.1016/j.jsames.2023.104314

In this study, we use seismic reflection and borehole data from the southeastern portion of Campos Basin to map and date igneous sills and volcanoes, and to assess how salt-tectonic structures influenced their morphology and distribution. We identify 99 sills emplaced within latest Aptian-to-Maastrichtian strata, and 15 volcanoes within late Cretaceous-to-Paleogene strata, covering a total area of c. 8,300 km². We also map over 310 km² of a lava field and identified four hydrothermal vents. We then discuss the timing of the main tectonic and magmatic events shaping this portion of the basin, and the interaction between salt flow, its resultant structures, and the spatially related igneous products.

2. Geological Context

The Campos Basin is located on the southeastern Brazilian margin, offshore the states of Rio de Janeiro and Espírito Santo (Figure 1a) (Guardado et al., 1989; Winter et al., 2007). The basin formed in the Early Cretaceous due to opening of the South Atlantic Ocean (Szatmari, 2000). The basin is limited to the north by the Vitoria Arch, to the south by the Cabo Frio High (Figure 2a), to the east by oceanic crust, and to the west by exposures of crystalline basement rocks of the Ribeira Belt (Mohriak et al., 1989; Heilbron et al., 2000).

The Campos Basin is subdivided into three tectono-stratigraphic sequences: rift, sag, and passive margin (Figure 1b). The rift sequence (Valanginian – Early Aptian) initiated at ~135 Ma with intense volcanic activity and the emplacement of extrusive igneous rocks (Baksi, 2018), which are overlain by continental fluvial and lacustrine deposits (Winter et al., 2007). Rifting was associated with the formation of NE-SW-striking normal faults that bound horsts and grabens (Figure 2a) (Chang et al., 1992; Guardado et al., 2000). The sag sequence (late Aptian) initiated with deposition of lacustrine carbonate rocks, which are overlain by a thick (up to 2 km) salt layer formed in response to episodic marine-water influx through the Walvis Ridge volcanic high to the south (Davison et al., 2012). Salt was deposited during several

depositional cycles (anhydrite, anhydrite + halite, anhydrite + halite + potash salts, i.e., carnallite and sylvinite; Winter et al., 2007). The passive margin sequence (Albian – Present) marks the development of the mid-Atlantic ridge and the establishment of oceanic spreading (Winter et al., 2007). Sedimentation during this latter stage of basin development was initially characterized by the deposition of shallow-water carbonate rocks, which were subsequently overlain by pelagic and hemipelagic clastics (Figure 1b; Chang et al., 1992).

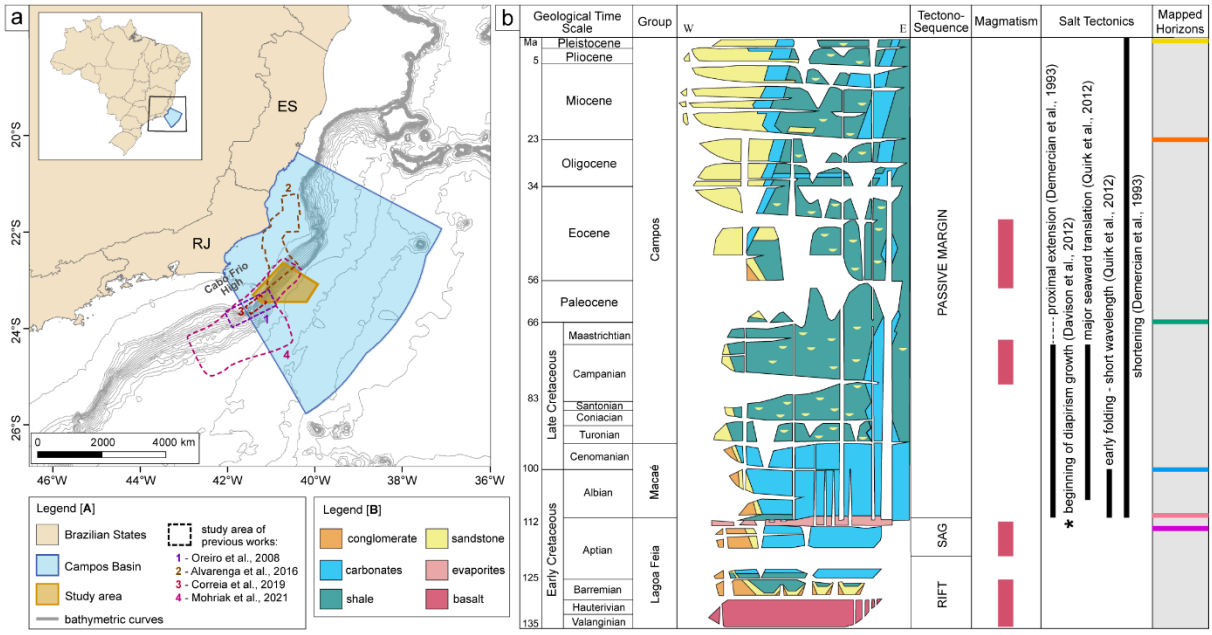

Figure 1. (A) Regional map showing the location of Campos Basin, our study area polygon and the study area of previous works. (B) Simplified stratigraphic chart of Campos Basin (redrawn from Winter et al., 2007), with the main magmatic events and timing of the salt tectonics from previous publications; the column to the right shows the mapped horizons of this study with their designed colours. The ages of the geological time scale are according to the International Chronostratigraphic Chart (Cohen et al., 2013).

2.1 Salt tectonics in Campos Basin

Salt-related deformation in the central South Atlantic region began in the late Aptian (i.e. *during* salt deposition) (Cobbold and Szatmari, 1991; Fiduk and Rowan, 2012; Davison et al., 2012), with the major seaward flow of salt and its overburden continuing until the Maastrichtian (Quirk et al., 2012). In the Campos Basin, salt (and its overburden) flowed across

Please cite as https://doi.org/10.1016/j.jsames.2023.104314

base-salt ramps, defined by variations in dip angle and direction in the base-salt surface, and which delineate the boundary between rift-related highs and lows (Amarante et al., 2021 – see their figure 4). Local areas of high strain at the top and base of such ramps, overprinted more regional patterns of salt-related deformation (Dooley et al., 2017). Based on the structural styles of the salt and its overburden, the Campos Basin is divided into three domains (Figure 2b): (i) a proximal extensional domain, associated with the formation of listric normal faults, rafts, and salt rollers; (ii) a distal compressional domain, containing salt-cored anticlines and diapirs; and (iii) an intermediate multiphase domain, with hybrid extensional/compressional structures and ramp syncline basins related to salt and overburden flow over base-salt relief (see above; see also Amarante et al., 2021). According to Amarante et al. (2021), the structures in the multiphase domain formed in response to multiple, kinematically-variable (extensional and contractional) phases of deformation that overlapped in time and space. These structures include: (i) contractional anticlines that were subjected to later extension and normal faulting; (ii) passively and actively rising diapirs that were later subjected to regional extension, developing landward-dipping normal faults on their landward flank; and (iii) an extensional diapir that was subsequently squeezed.

2.2 Magmatism in Campos Basin

The southeastern Brazilian basins (mainly the Campos and Santos basins) underwent four main magmatic events, two of them preceding salt deposition (i.e. rift and sag stages; Barremian – Aptian), during 130 – 120 Ma and c. 118 – 112 Ma, both characterized by tholeiitic to intermediate dykes, flood basalts and intrusions (Winter et al., 2007). Alvarenga et al. (2016) identified hydrothermal vents in the southern Campos Basin (Figure 1a), in the syn-rift and sag stages. The authors described 10 hydrothermal vents, seven with dome-shaped geometries and

Please cite as https://doi.org/10.1016/j.jsames.2023.104314

three with eye-shaped geometries, all of which were associated with the two Early Cretaceous magmatic episodes (Figure 1b).

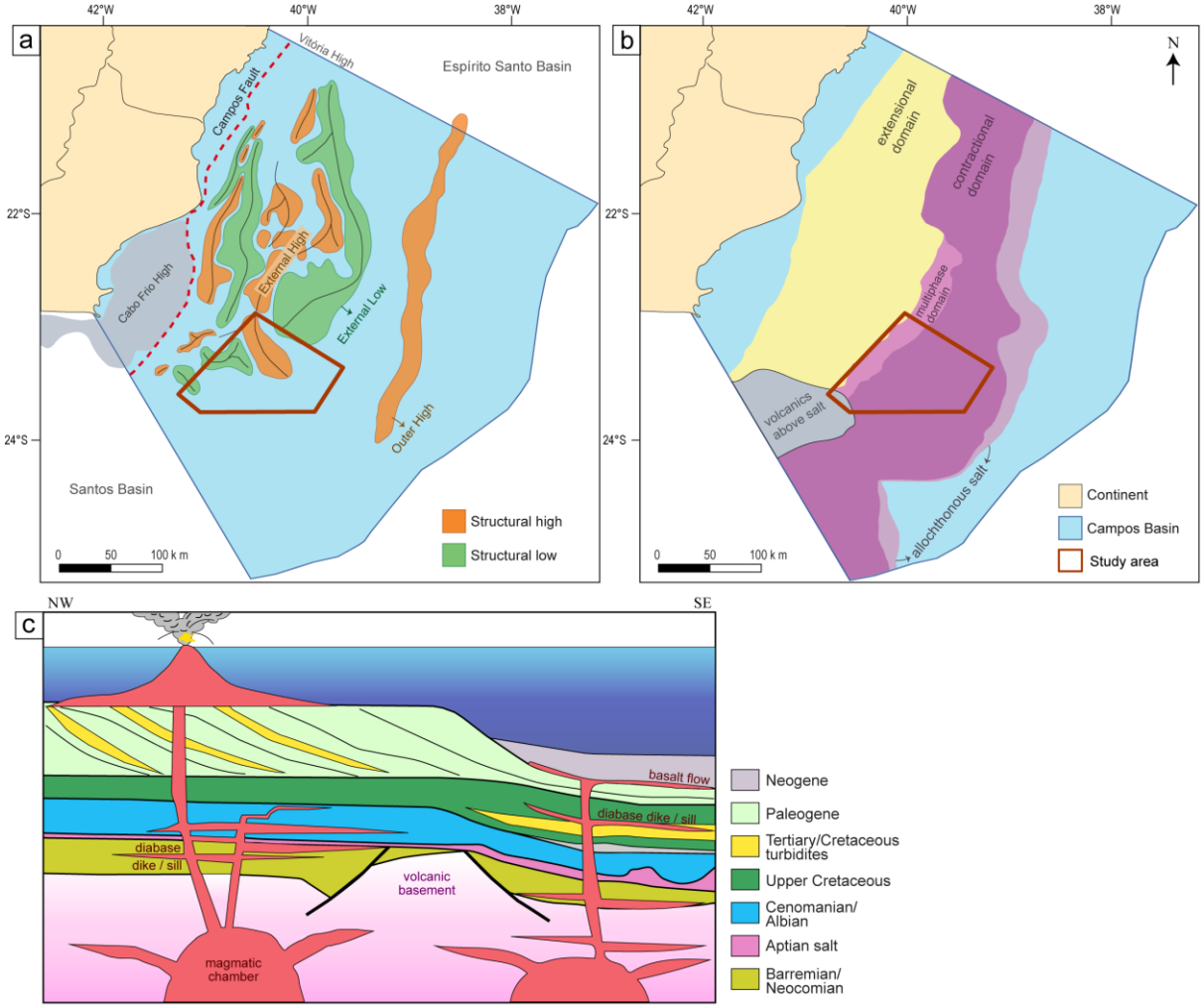

Figure 2. (A) Rift-related structural framework of Campos Basin, redrawn from Guardado et al. (2000); Outer High and Cabo Frio High locations from Fetter (2009). (B) Salt-related structural provinces, modified from Davison et al. (2012) and Amarante et al. (2021); the location of the *volcanics above salt* (or Cabo Frio Volcanic Province, according to Mohriak et al., 2020) is from Meisling et al. (2001). (C) Schematic cross section showing the Late Cretaceous to Paleogene magmatic events in the Campos Basin (redrawn from Mohriak et al., 2020).

Immediately after salt deposition (late Aptian, c. 116 – 111 Ma), igneous extrusions and intrusions were emplaced during several magmatic pulses across southeast Brazil, from the late Upper Cretaceous to the Early Paleogene (Figure 2c), particularly during c. 60–40 Ma and c. 80–70 Ma (Figure 1b; Oreiro, 2006; Moreira et al., 2006; Thomaz Filho et al., 2008; Ren et al., 2019). By quantifying the percentage of volcanic fragments in different deep-water reservoirs

Please cite as https://doi.org/10.1016/j.jsames.2023.104314

of the Campos Basin, Fetter et al. (2009) suggested that the climax of volcanism occurred in the Late Maastrichtian. The Late Cretaceous to Paleogene magmatic episode emplaced a cluster of magmatic products in the Cabo Frio Volcanic Province (e.g. volcanics above the salt in Figure 2b), located between Campos and Santos basins, with volcanic build-ups, dykes, saucer-shaped sills, and lava flows intercalated within the deep-water sedimentary sequences (see Mohriak et al., 2021 and references therein).

Oreiro et al. (2008) identify post-Aptian (Late Cretaceous and Tertiary) volcanic edifices, lava flows, feeder dikes, and sills in the southern Campos Basin – northern Santos Basin region (Figure 1a). According to these authors, the related post-salt magmatic events resulted from the reactivation of deep-seated, NE-SW-striking fault zones, many of which formed to accommodate the breakup of the Pangaea supercontinent. This interpretation is supported by the observation that the volcanic features are aligned with the main faults and are more abundant in regions with higher fault density (Oreiro et al., 2008).

Correia et al. (2019) mapped 15 sills in the southern Campos Basin (Figure 1a), between the Albian and top Eocene, product of four magmatic events: early Campanian, early Paleocene and early- and mid-Eocene. They described five types of sills based on their 3D geometry: saucer-shaped, slightly saucer-shaped, climbing saucer-shaped, transgressive, and rough layer-parallel. The areas of the described sills vary from 0.82 to 14.35 km², with the long axis ranging from 1.01 to 6.82 km (Correia et al.,2019).

Mohriak et al. (2021) document igneous products from the four aforementioned magmatic events (Valanginian-Barremian, Aptian, Campanian-Maastrichtian, Paleocene-Eocene; see Figure 1b) in the Cabo Frio High region (i.e., southern Campos Basin – northern Santos Basin) (Figure 1a), focusing on their influence on oil and gas systems. They describe extrusive (e.g. lava flows and volcanoes) and intrusive (e.g., sills) at various stratigraphic levels.

Please cite as https://doi.org/10.1016/j.jsames.2023.104314

Fiduk et al. (2004) describe igneous products and their relationship to the underlying salt structures in the Espírito Santo Basin. These authors show igneous intrusions (mostly saucer-shaped sills) and feeder dikes emplaced in Albian and Late Cretaceous strata, and extrusive lava flows erupted along the Cretaceous – Paleogene boundary. The lava flows appear to have erupted from the basinward flank of a large salt-detached anticline, and to have flowed towards the adjacent syncline (Fiduk et al., 2004). According to these authors, there is a higher occurrence of igneous intrusions above or adjacent to the underlying salt structures because intruding magmas preferentially used salt structures and associated faults as ascent pathways.

Magee et al. (2021) mapped 38 igneous intrusions in the proximal southeastern Santos Basin. The authors classify the intrusions based on their geometries, i.e. sub-horizontal sills, saucer-shaped sills, and inclined sheets. From the 38 interpreted structures, 18 are located above the salt, 18 within the salt, and two below the salt. Most of the intrusions above the salt occur within the Turonian and the Coniacian (c. 86 – 94 Ma). The area of the mapped supra-salt intrusions (dominantly saucer-shaped) vary from 1.9 to 21.9 km², with the long axis of individual intrusions varying from 2.22 to 6.42 km. The intra-salt intrusions (mostly inclined sheets and saucer-shaped sills) vary in area from 1.6 to 15.1 km², with long axis from 1.99 to 5.8 km (Magee et al., 2021 – see their table 1). Through seismic-stratigraphic relationships between the igneous products and the surrounding strata, the authors interpret magmatism occurred between the Albian and Santonian, synchronous with gravity-driven salt tectonics. Magee et al. (2021) suggest that at their time of their emplacement, the igneous products enhanced salt flow, but after their cooling and crystallization, they inhibited salt movement, which ultimately influenced the style and evolution of salt deformation and in particular, diapirism.

Please cite as https://doi.org/10.1016/j.jsames.2023.104314

3. Database and Methodology

Our seismic reflection database comprises 60 2D lines and one 3D volume from the ANP (Brazil's National Oil, Natural Gas and Biofuels Agency) data library, covering an area of c. 8,300 km² of the southwest portion of Campos Basin (Figures 1a and 3). The 3D volume covers an area of c. 2,900 km², with inlines (east-west) and crosslines (north-south) spaced 12.5 m (Figure 3). The seismic surveys are time-migrated (PTSM Kirchoff), zero-phase processed, with a display following SEG "normal" polarity; i.e. a downward increase in acoustic impedance is represented by a positive reflection event (i.e. red on displayed seismic profiles), whereas a downward decrease in acoustic impedance is represented by a negative reflection event (i.e. blue on displayed seismic profiles). All seismic data (lines and maps) are presented in two-way travel time (TWT) milliseconds (ms).

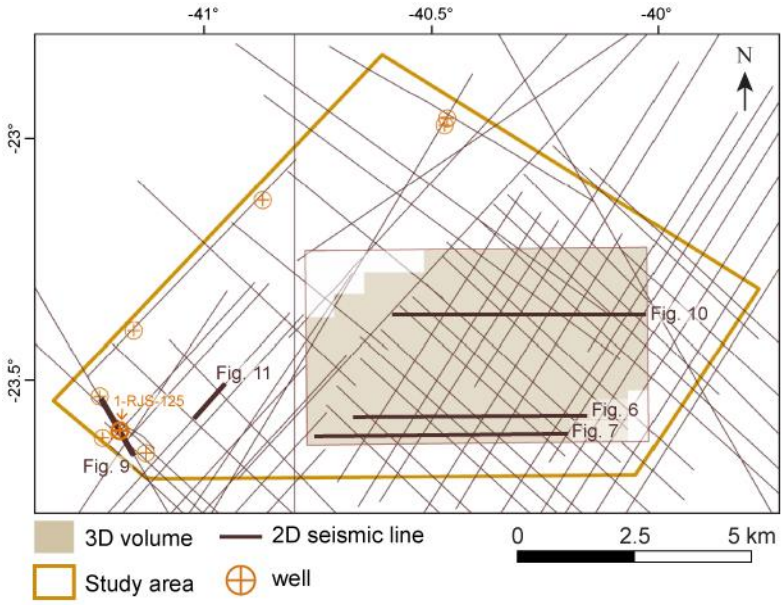

Figure 3. Dataset used in this study: 60 2D seismic lines (or lines segments), one 3D volume and 8 boreholes from the ANP data library. The seismic lines shown in figures 5, 6 and 7 are labelled, and also the well 1-RJS-125 shown in figure 11.

Within the study area there are eight boreholes that contain well-logs (e.g. sonic travel time, bulk density, and gamma ray), and stratigraphic (i.e. age) and lithology data that help us constrain the age of the mapped horizons and igneous products, and the composition of the

Please cite as https://doi.org/10.1016/j.jsames.2023.104314

interval of interest. The names of the boreholes are: 1-RJS-0166, 1-RJS-0433, 1-RJS-0125, 1-RJS-0498, 1-RJS-0365, 1-RJS-0504, 3-BRSA-304 and 3-BRSA-0255.These wells were tied to the seismic data through checkshot surveys. The interval velocity of the Aptian evaporites obtained from the well-logs ranges from 4000 – 7000 m/s, depending on the proportion of halite, anhydrite, and potash salts. The overlying Albian interval, composed mainly of carbonates, is defined by interval velocities ranging from 3000 – 6000 m/s. The Cenomanian to Recent succession is defined by interval velocities ranging from 1800 – 3000 m/s. The wide variation in interval velocities in the sedimentary rocks above the salt is due to the highly varying densities and porosities of the different lithologies (e.g. mudstone, sandstones, conglomerates, carbonates). Only one well (1-RJS-0125) constrains the interval velocity of the mafic extrusive igneous rocks, 4700 m/s, which we use to calculate the height of the volcanoes. This value is lower than those previously reported for comparable mafic rocks (i.e., 5500-6600 m/s), perhaps because the Campos Basin examples have been weathered and/or the initial melt was particular gaseous, resulting in vesicle-rich deposits (Planke et al., 2000, 2005; Mark et al., 2018). We estimate that the vertical seismic resolution in the interval of interest is 10 – 50 m. More specifically, 30 – 50 m within the salt layer and 10 – 40 m within the overlying Albian carbonates (considering a dominant frequency of 35 Hz), 10 – 15 m within the Cenomanian to Recent sedimentary strata and 20 – 25 m within the volcanoes (considering a dominant frequency of 50 Hz).

We mapped five key horizons across the seismic dataset: base of salt, top of salt, top Albian, top Cretaceous and top Paleogene (Figure 1b). We chose the top Albian, top Cretaceous and top Paleogene horizons because they represent regional seismic-stratigraphic unconformities that are easily identifiable throughout the Campos Basin, record major periods of salt-related deformation, and constrain the age of the volcanic products. We mapped 99 igneous intrusions and 15 volcanoes based on seismic facies analysis, i.e. amplitude, polarity, lateral continuity, internal configuration and external geometry. The interpreted volcanoes have

conical geometries and are characterized internally by chaotic seismic facies. One volcano in our study area is penetrated by a well (1-RJS-125; Figure 3). Sills are expressed as high-amplitude, laterally discontinuous (on a kilometer scale) reflections that are often discordant with surrounding stratigraphic reflections (Planke et al., 2005). Sills are invariably defined at their tops by a positive reflection event, defining a downward increase in acoustic impedance. Near the top-salt horizon we could not confidently map concordant sills, given they have a similar seismic expression to Albian carbonates. The sills in our study area are not penetrated by wells, although they have very similar seismic expressions to the ones documented by Correia et al. (2019), noting that those authors document 14 sills, penetrated by and compositionally constrained by 7 wells, in a study area that is close to and partially overlaps with ours (Figure 1a). Correia et al. (2019) interpret the intrusions as mafic, being characterized by low-silica content, and low GR values (21–34 gAPI) due to their lack of radioactive minerals. We classified the interpreted sills according to their geometries, following Planke et al. (2005): saucer-shaped, planar, transgressive, layer-parallel, and fault block. Thin intrusions, with thickness below the detection limit or limit of visibility, may not be imaged by our seismic reflection data (Eide et al., 2018). Surface and thickness maps were generated for the 3D volume, aiming to analyze the relation between the igneous products and salt tectonics.

Please cite as https://doi.org/10.1016/j.jsames.2023.104314

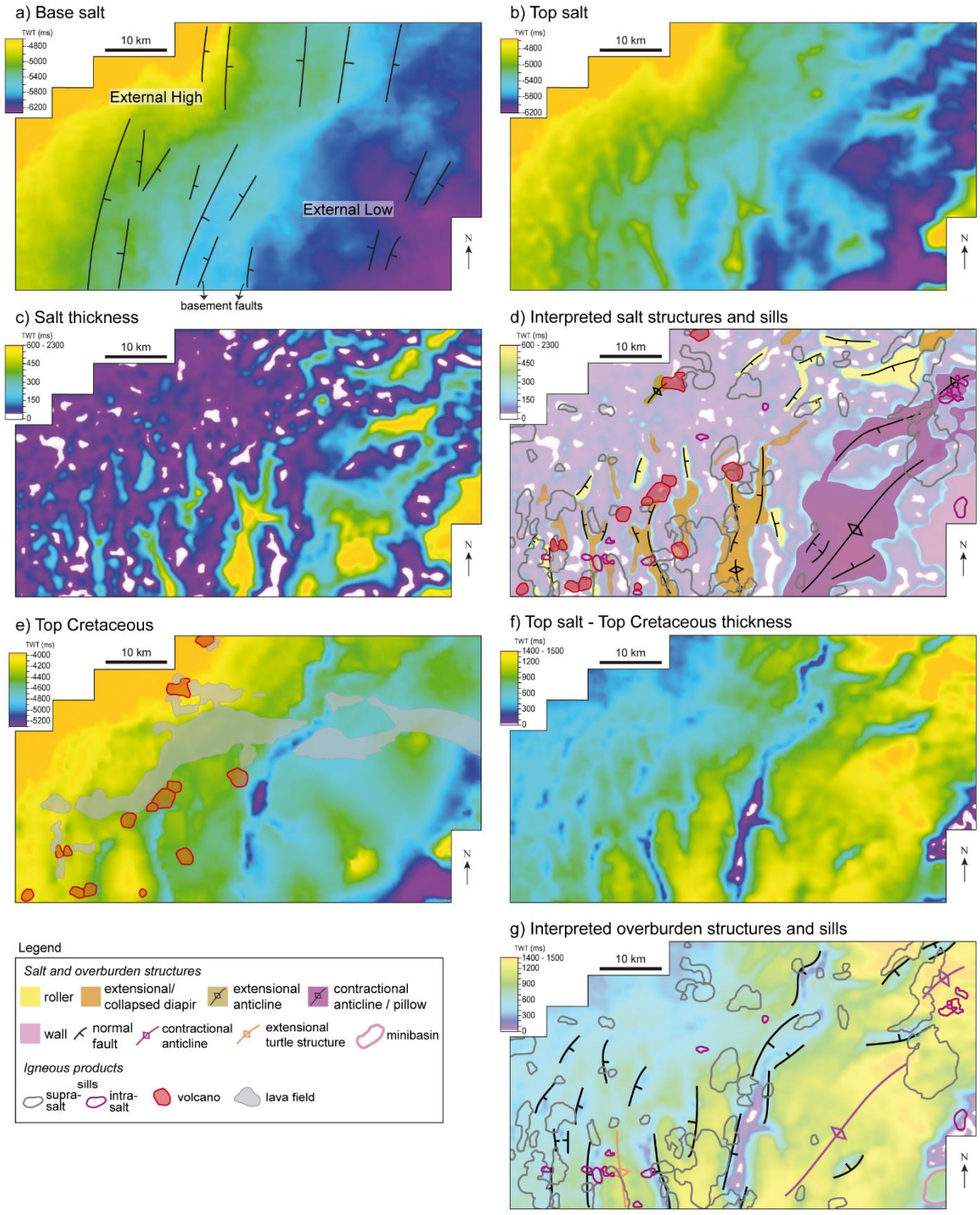

Figure 4. Time maps of the 3D volume. a) Base-salt surface map, which vary from -3900 to -6400 ms (TWT), with the underlying basement faults and structures (External High and External Low; Guardado et al., 2000). b) Top-salt surface map, ranging from -4500 and -6300 ms (TWT). c) and d) show salt isochron thickness map, with values ranging from 0 to 2500 ms (TWT) defining salt welds and salt structures, interpreted in (d). e) Top Cretaceous surface map, varying from -3600 and -5500 ms (TWT), with the interpreted volcanoes and lava flows (see figure 8c). f) and g) show the isochron thickness map between the top salt and top Cretaceous, which varies from 0 to 1500 ms (TWT), defining overburden structures interpreted in (g).

Please cite as https://doi.org/10.1016/j.jsames.2023.104314

4. Results

4.1. *Sub-salt structures*

The base-salt surface dips regionally to the SE (Figure 4a). It is shallowest to the west, defining the External High, deeper to the east, defining the External Low, and is characterized by numerous rift-related, basement-involved structures that are separated by N-S- to NNE-SSW-striking normal faults. The base-salt surface is rugose, with ramps that reflect the complex underlying topography – the largest ramp defines the boundary between the External High and External Low (Figures 5, 6 and 7).

4.2. *Salt structures*

The top salt surface varies in depth between 4500 and 6300 ms TWT (Figure 4b). Salt thickness is highly variable (0-2400 ms TWT; Figure 4c), defining salt structures and salt welds, i.e. areas of relatively thin, depleted salt (white areas on Figure 4c). The main salt structures are elongated, reaching up to 37 long 15.5 km wide, that trend broadly NE to N (Figure 4d). In the western portion of the study area (on and adjacent to the External High), salt forms several rollers and collapsed diapirs that are associated with overburden normal faults. Salt structures in the east of the study area (on and adjacent to the External Low) include an extensional salt roller, and several diapirs (one of which has undergone extensional collapse, developing a crestal graben) and shortening-driven salt anticlines (Figure 4d). Some of these structures are geometrically and kinematically complex, given they formed in response to multiple phases of extension and contraction that overlapped in time and space (see Amarante et al., 2021).

Please cite as https://doi.org/10.1016/j.jsames.2023.104314

4.3. *Supra-salt structures*

Key overburden structures are displayed on the Top Salt to Top Cretaceous isochron map (Figure 4f, g). The top Cretaceous varies between 3600 and 5500 ms TWT depth (c. 8 to 12 km; Figure 4e), and the top salt to top Cretaceous interval varies in thickness from 0 to 1500 ms TWT (Figure 4f). The interpreted overburden structures have broadly the same orientation as underlying salt structures, and where the underlying salt has pierced the entire Cretaceous succession the latter is absent (white areas in Figure 4f,g). On and adjacent to the External High, salt rollers and collapsed diapirs are associated with overburden normal faults that delimit grabens, extensional rollovers, extensional turtle structures (i.e. extensional anticlines), and Albian rafts (Figures 5, 6, 7 and 4g). On and adjacent to the External Low, the overburden is defined by anticlines, a minibasin (Figure 4g), and normal faults (e.g. Figure 5) that can define small grabens (Figure 6) and extensional rollovers (Figure 7); we also interpret a ramp syncline basin (RSB, Figure 7) between the Albian and top Cretaceous horizons. Growth strata associated with salt-detached normal faults and salt anticlines indicate that both extensional and contractional deformation was more significant from the Albian to the top Cretaceous than during the Paleogene (Figures 5, 6 and 7).

Please cite as https://doi.org/10.1016/j.jsames.2023.104314

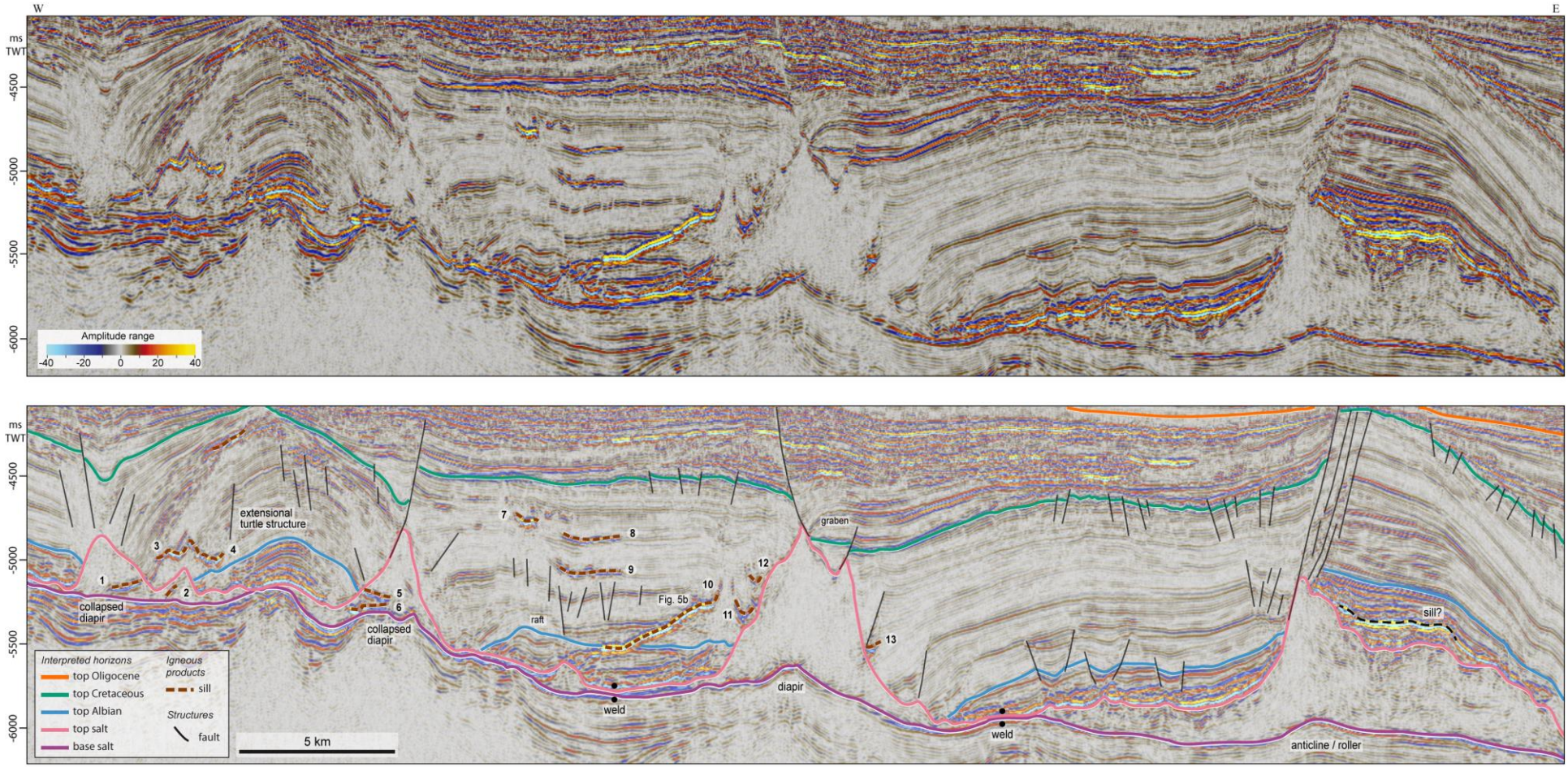

Figure 5. Inline seismic section (W-E). The lower section shows the interpreted seismic horizons, sills and faults. The sills are numbered to facilitate indications in the text. The main salt and overburden structures are labeled. See figure 3 for location. Seismic data supplied by ANP.

Please cite as https://doi.org/10.1016/j.jsames.2023.104314

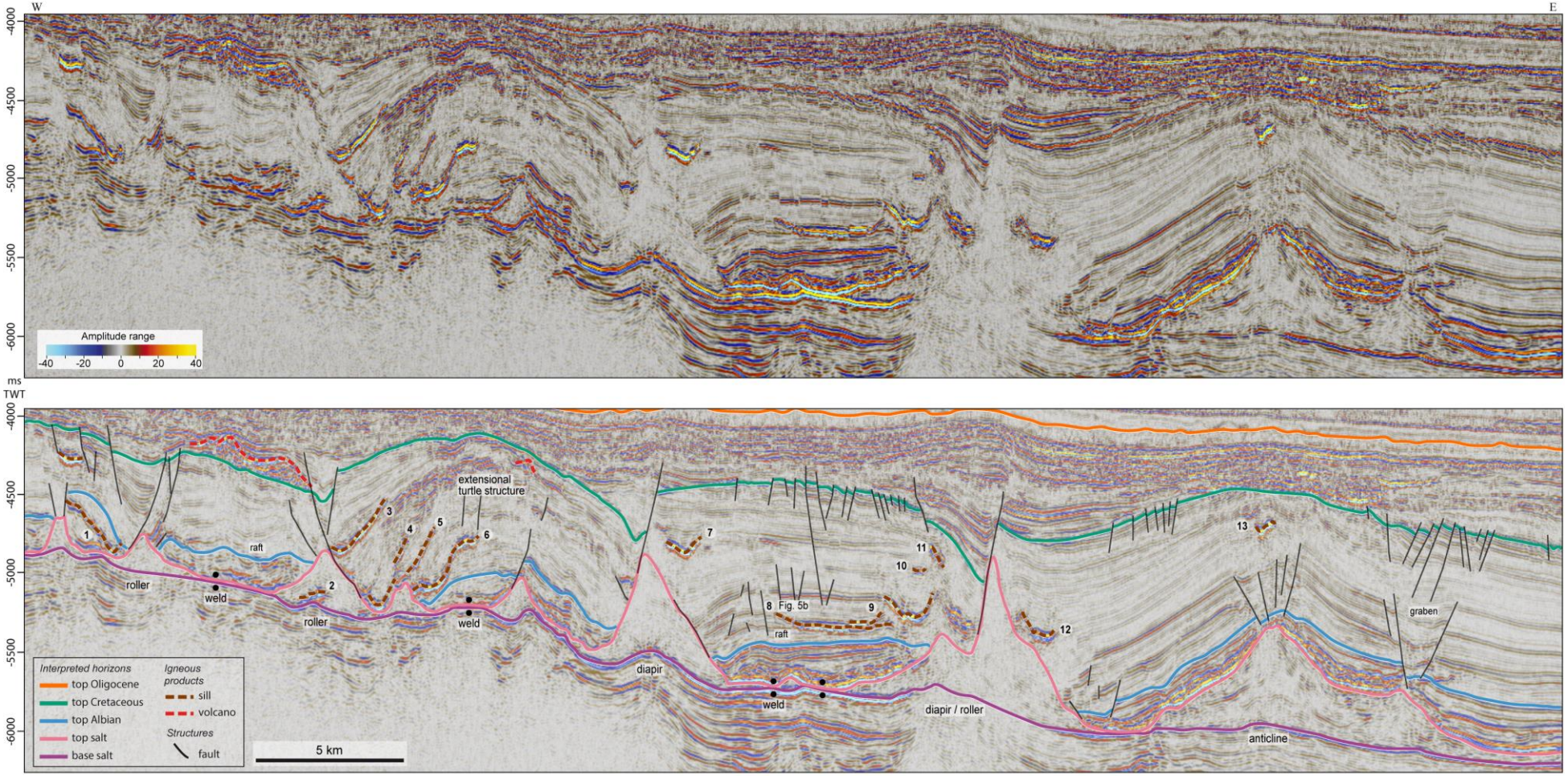

Figure 6. Inline seismic section (W-E). The lower section shows the interpreted seismic horizons, igneous products and faults. The sills are numbered to facilitate indications in the text. The main salt and overburden structures are labeled. See figure 3 for location. Seismic data supplied by ANP.

Please cite as https://doi.org/10.1016/j.jsames.2023.104314

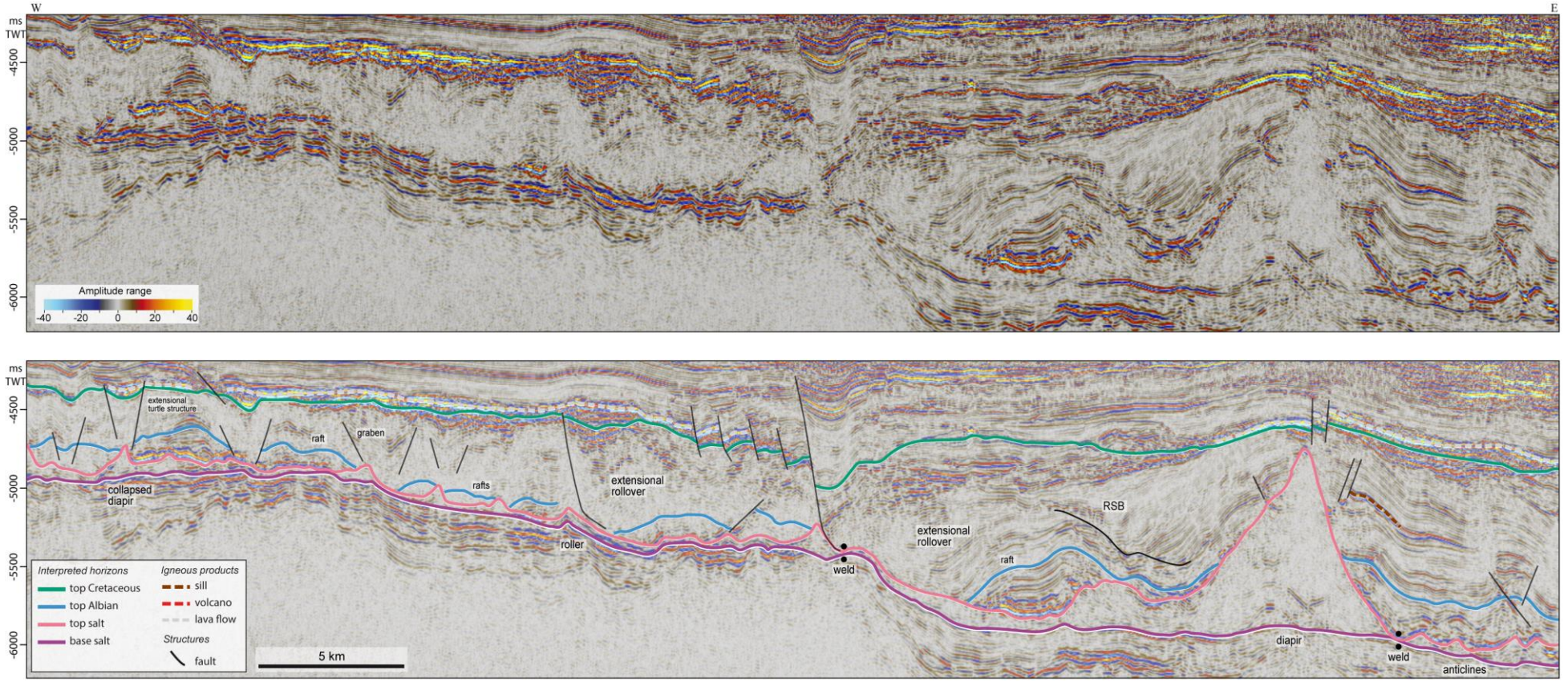

Figure 7. Inline seismic section (W-E). The lower section shows the interpreted seismic horizons, igneous products and faults. The sills are numbered to facilitate indications in the text. The main salt and overburden structures are labeled. See figure 3 for location. Seismic data supplied by ANP.

Please cite as https://doi.org/10.1016/j.jsames.2023.104314

4.4. *Igneous products*

a. Sills

We mapped 99 sill-like intrusions (Figure 8a,b). The intrusions have long axes ranging from 0.4 to 14.3 km, areas between 0.1 and 57 km², and are sub-circular to elongate in plan-view. They are located mostly in the southern part of the study area, being more numerous in the southern and southwestern portions of the 3D seismic volume (Figure 8a,b). Of the 99 mapped intrusions, 83 are emplaced above the salt and 16 are intra-salt (Figure 8a,b). The sills above the salt mainly occur in strata between the Albian and top Cretaceous horizons (Figures 9, 5 and 6), although some are emplaced in Albian strata (Figures 9b and 6 to the W). Igneous intrusions occur mainly on and adjacent to the External High, where salt tectonics is characterized by extensional structures, mainly rollers and collapsed diapirs that are associated with normal faults, grabens, and extensional rollovers (Figures 9d,g).

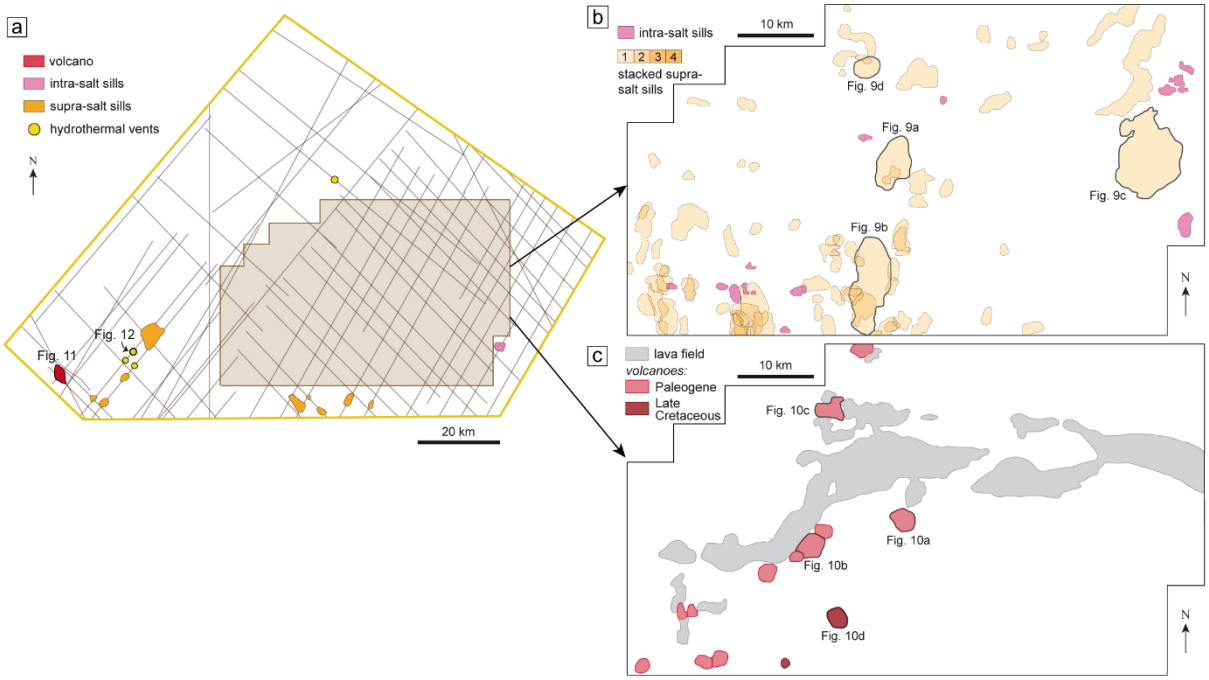

Figure 8. (a) Interpreted volcanic field, hydrothermal vents, intra-salt sill and supra-salt sills on the 2D seismic data; (b) interpreted intra-salt and supra-salt sills on the 3D volume; (c) interpreted volcanoes and lava field on the 3D volume. The igneous products shown in figures 9, 10, 11 and 12 are labelled.

Please cite as https://doi.org/10.1016/j.jsames.2023.104314

Intra-salt sills are found in different types of salt structures: diapirs, anticlines, and extensional rollers, in which salt thickness varies from 150 to 2000 ms (TWT) (Figure 9d). Most intra-salt sills occur to SW and E of the 3D volume and are commonly isolated, rather than forming interconnected sill-complexes (Figure 8b). Supra-salt sills occur mostly where salt is relatively thin (0 – 550 ms TWT), in the extensional domain where extensional diapirs and rollers dominate, and overburden normal faults, grabens, and extensional anticlines are common (Figure 9d,g). Sometimes supra-salt sills are spatially coincident with normal faults normal faults (Figure 9a,d; Figure 6 sills 3 – 6, Figure 10a,a1). In contrast to the intrasalt sills, most supra-salt sills are interconnected, forming sill-complexes, occurring mainly in the SW of the 3D volume (Figure 8b). The distribution of intra- and supra-salt sills (Figures 8b and 9d) show they do not spatially overlap.

We identified three types of intrusions: saucer-shaped, planar transgressive, and layer-parallel (*sensu* Planke et al., 2005). Saucer-shaped sills have arcuate geometries in cross-section, displaying sub-horizontal-to-flat centers and peripheral inclined limbs that cross-cut the overlying stratigraphy (e.g. Figure 9a,d, Figure 6 sills 7 and 9). Figure 9a shows the 3D geometry of a saucer-shaped sill that was emplaced in the fault planes that delimit a salt-related graben (Figure 9a1). This sill is emplaced within Upper Cretaceous strata, with the eastern limb extending up to just below the Top Cretaceous horizon. It measures 7 x 4.2 km (long and short axes), extends 600 ms (TWT) or c. 540 – 600 m vertically, and has an area of 17.7 km². Figure 9d presents another example of a saucer-shaped sill, emplaced between early Albian – top Cretaceous strata, towards the late Cretaceous as indicated by a forced fold above the sill (Figure 9d1). This sill measures 3.2 x 2.8 km (long and short axes) and has an area of 5 km². Planar transgressive sills extend upwards and crosscut the stratigraphy in a staircase-like manner (e.g. Figure 5 sill 4, Figure 6 sills 4, 5 and 6). Figure 9b shows the largest transgressive sill in the study area, which cross cuts the stratigraphy from the early Albian to the mid-Upper-Cretaceous (Figure 9b1) at angles of up to 26°, extending vertically 500 ms (TWT). This sill

has an area of 37.5 km² and measures 12.4 x 4.7 km (long and short axes). Layer parallel sills are strata-concordant, occasionally with transgressive segments (e.g. Figure 9c, Figure 5 sill 9, Figure 10a sill 2). Figure 9c shows a layer parallel sill emplaced within upper Cretaceous strata (Figure 9c1), measuring 11 x 8 km (long and short axes), and with an area of 57 km². It is important to note that this feature is a sill rather than a carbonate build-up because its emplacement is post-Albian, i.e. deep-water sedimentation consisted of marls and shales (Winter et al., 2007).

Intra-salt sills do not present a clear stratigraphic relation to the surrounding strata, given the chaotic seismic facies of the salt; they are thus classified as sub-horizontal (e.g. Figure 5 sills 5 and 6) or inclined sheets (e.g. Figure 5 sills 1 and 2; Figure 6sill 2). Intra-salt sills are not as big, in terms of their long-axis length and area as the supra-salt sills, having long axes of 0.4-3 km and areas 0.1-3.2 km².

Please cite as https://doi.org/10.1016/j.jsames.2023.104314

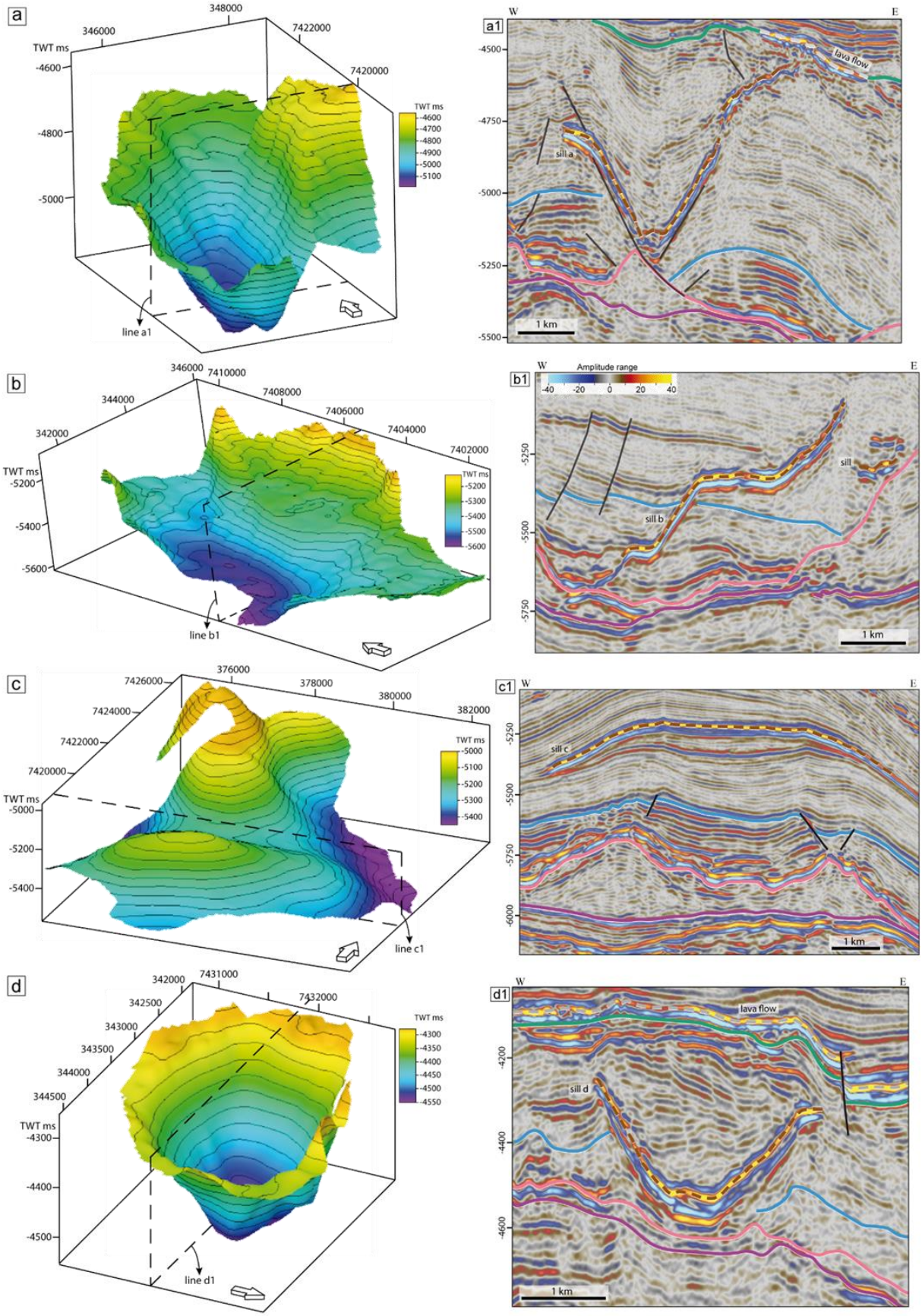

Figure 9. (a) 3D view of a saucer-shaped (locally fault block, see Figure 9a1) (b) 3D view of a planar transgressive sill; (c) 3D view of a layer parallel sill; (d) 3D view of a saucer-shaped sill. a1, b1, c1 and

Please cite as https://doi.org/10.1016/j.jsames.2023.104314

d1 show inlines seismic sections (W-E) highlighting the geometries of the selected sills. See figure 8d for their location.

b. Volcanoes

We identified 15 volcanoes in the study area (Figure 8a,c). The volcanoes are largely restricted to the western part of the 3D seismic volume, where they are aligned in chains that trend NE, although a single volcano is identified further west on a single 2D seismic profile. The volcanoes occur mainly in the Lower Paleocene interval (Figures 6, 10a-c and 11a) at the same stratigraphic level, except for two that occur in uppermost Cretaceous rocks (Figures 6 and 10d). The volcanoes have basal diameters of 2.4-7.2 km (mean 4.6 km), and are 210-940 m (mean 500 m) tall. They typically display conical shapes, which are internally characterized by chaotic seismic facies, and are weakly to moderately reflective, with distinct reflections downlapping towards the reflection bounding their base. The flanks of the volcanic cones are defined by high-amplitude reflections (Figure 10b-d) that are onlapped by overlying strata (Figures 10 and 11a). Below the volcanoes there are slight pull-ups of underlying reflections, which we relate to the igneous rock-dominated volcanoes being characterized by faster velocities than adjacent, encasing sedimentary strata (best seen in Figure 10b-d). Underlying reflections (from directly below the volcano to at least the top Albian) are also typically of relatively low-amplitude and are discontinuous (Figure 10); an exception is shown in Figure 10a1, where directly below the volcano there are high-amplitude reflections, that could be interpreted as feeder intrusions.

Please cite as https://doi.org/10.1016/j.jsames.2023.104314

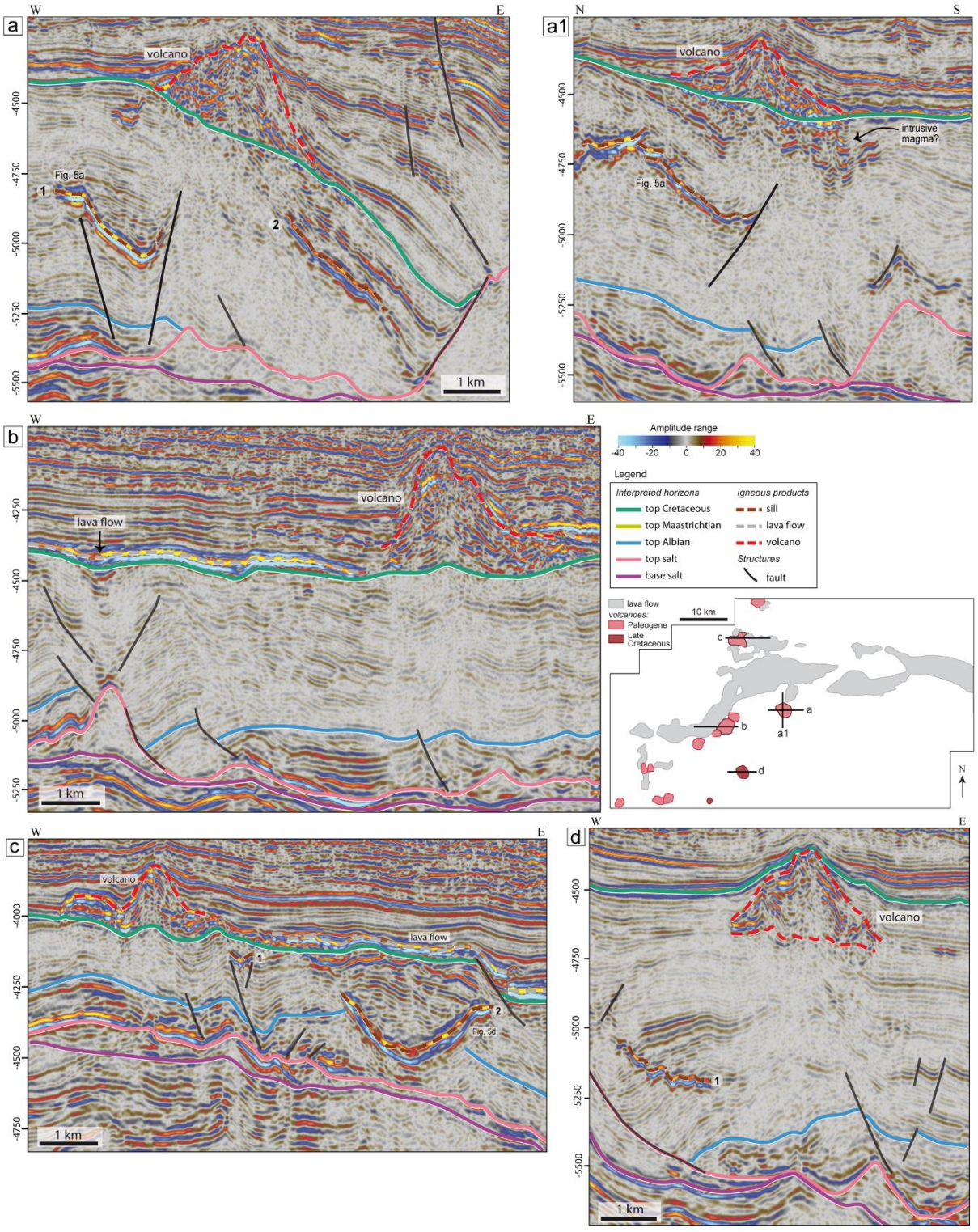

Figure 10. Seismic sections showing interpreted volcanoes in the 3D volume, with the interpreted horizons, lava flows and sills. (a), (b) and (c) show Paleogene volcanoes, and (d) shows an upper Cretaceous volcano. Note that the volcanoes typically present a conical shape. See map in the left for the seismic sections location.

The gamma-ray curve of well 1-RJS-125 suggest two distinct compositions for igneous rocks in the Campos Basin (Figure 11b). The Upper Cretaceous igneous rocks (Cenomanian –

Please cite as https://doi.org/10.1016/j.jsames.2023.104314

Maastrichtian) present higher gamma-ray values (average of 65) and have been previously described as basaltic lava flows (Mohriak et al., 2021). In the seismic data, these rocks are characterized by a positive, high-amplitude, continuous (over 7 km) reflection (Figure 11a). The overlying Paleogene igneous rocks have lower gamma-ray values (average of 30), which when combined with the conical geometry and internal chaotic seismic facies, suggest they constitute a pyroclastic cone composed of hyaloclastites and tuffs build-ups above the lava flows (Mohriak et al., 2021).

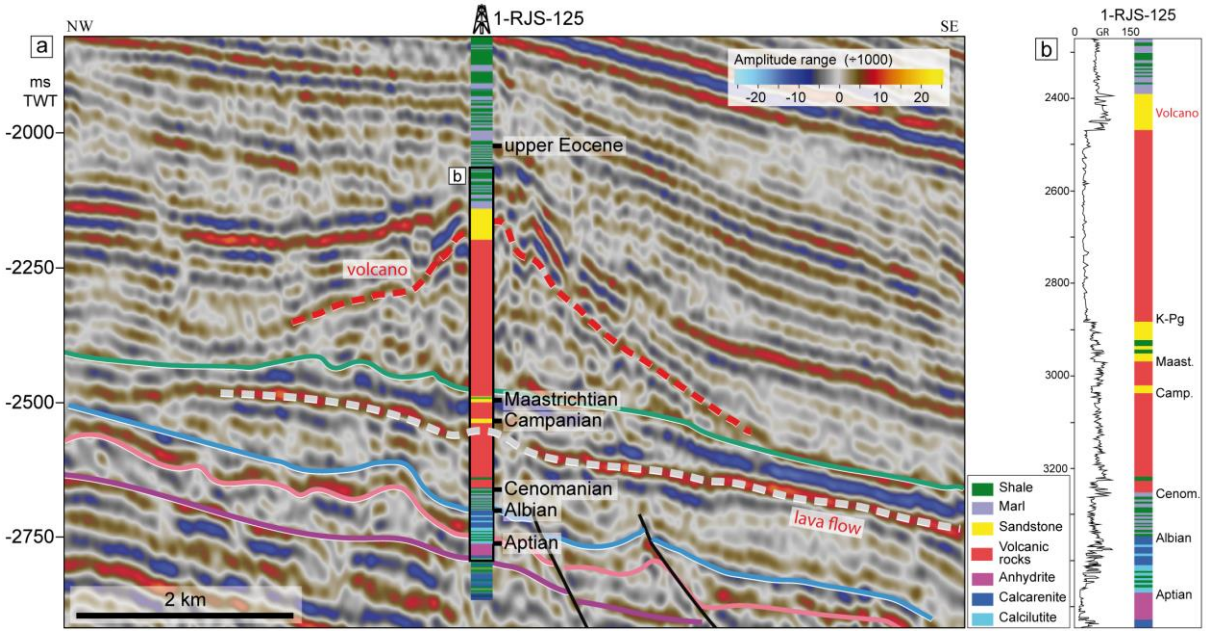

Figure 11. (a) Seismic line showing the well 1-RJS-125 drilled through a volcano, with the positions of the ages Aptian, Albian, Cenomanian, Campanian, Maastrichtian (top Cretaceous) and upper Eocene; the top of the volcano is indicated by a red dashed line. (b) Lithology and gamma ray curves of the well 1-RJS-125. These are also shown in Mohriak et al., 2021 (see their figure 20).

c. Lava field

We interpreted a lava field extending for at least c. 310 km² within the 3D seismic volume (Figure 8c). The field is characterized by a 40 – 100 ms (TWT) (c. 100 to 280 m) thick package of high-amplitude reflections that generally occur adjacent to a volcano; the top of the package is defined by a strong, continuous, positive reflection, which defines a downward

Please cite as https://doi.org/10.1016/j.jsames.2023.104314

increase in acoustic impedance. The lava field is separated into discrete areas, the larger ones located at the center-north of the 3D volume, where sills are less numerous (Figure 8). Like the Paleogene volcanoes, the interpreted lava flows overlie the top Cretaceous horizon, being concordant with the underlying reflections (Figures 10b,c and 7). Reflections underlying the lava fields are typically discontinuous and are of lower amplitude than the igneous rock-bearing unit, especially where the associated extrusive igneous rock successions are thicker (Figure 10). We observe local changes in the thickness of lava fields associated with salt-related relief, i.e. they are thicker in lows than they are across adjacent highs (Figure 7). The lava fields are elongate and trend N, NE, or E trends (Figure 8c). Lava fields have been previously documented in the southwest Campos Basin, where they also overlie the top Cretaceous reflection (Oreiro et al., 2008).

We also identified four vent-like structures (Figure 8a). These are defined by a lower, seismically chaotic part, which we infer may be a conduit for rising fluids, gas, and rock material expelled from the vent (*sensu* Planke et al., 2005), and an upper, dome- or eye-shaped part that is the vent edifice. Figure 12 shows an example of a Paleogene-hosted vent-like structure that is underlain by a c. 915 ms (TWT) tall conduct that appears to emanate from a sub-salt sill complex. The conduit itself is characterized by disrupted, upward-deflected reflections. The vent itself has a basal diameter of c. 850 m, is c. 90 ms TWT tall, and it is internally characterized by outward-dipping reflections that concordant with the vents upper surface and that downlap the reflection defining the vent base. Vent-like structures were only identified in the 2D seismic data, three of them in the SW and one to the NE of the study area. The vents and underlying conduits in SW occur in the same stratigraphic level (sub-salt – Paleogene; Figure 12), whereas the vent and underlying conduit to NE occurs from the sub-salt to the Upper Cretaceous (measuring c. 550 ms TWT tall).

Please cite as https://doi.org/10.1016/j.jsames.2023.104314

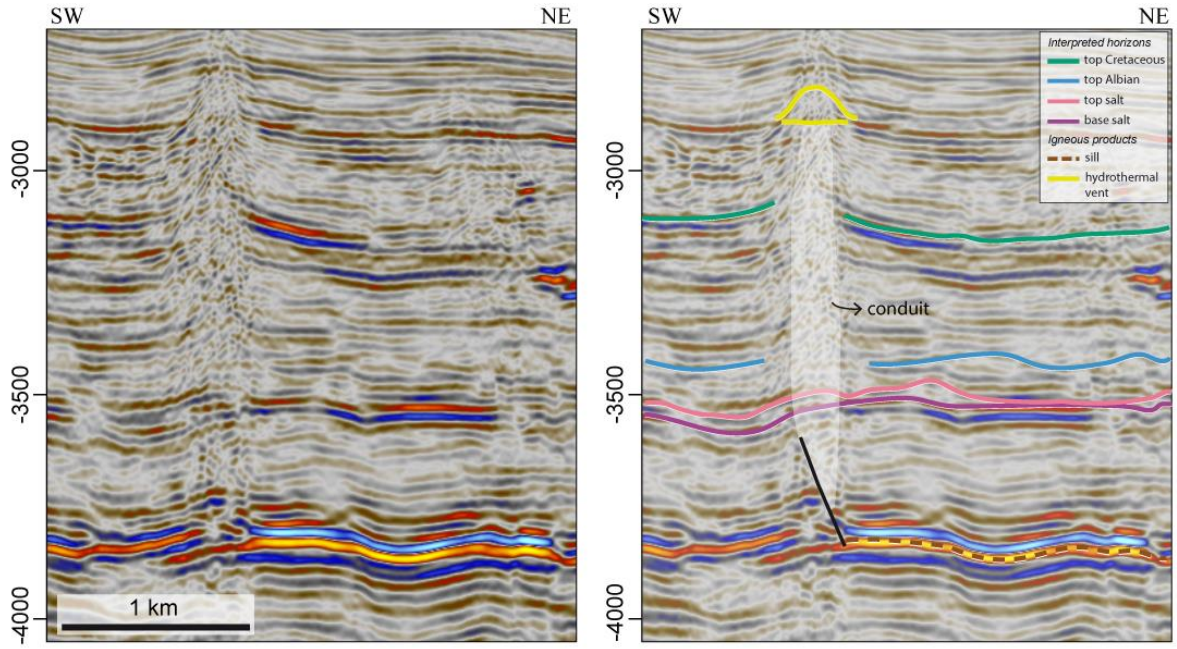

Figure 12. Uninterpreted (left) and interpreted (right) seismic section, showing the interpreted seismic horizons, sill and hydrothermal vent.

5. Discussions

5.1. *Timing of igneous activity*

We mapped 99 sills in the study area, 16 intra-salt and 83 above the salt, between the top Albian and top Cretaceous horizons and, more rarely, within Albian strata (e.g. Figure 6). Due to the lack of borehole data and more specifically radiometric data from rock samples, we do not directly know the precise timing of sill emplacement and related magmatism. However, the age of the sill host rock defines the maximum sill age, thus the oldest sills were emplaced during magmatic activity between the late Aptian (i.e., the age of the salt) and the end of the Cretaceous. Again, due to a lack of radiometric age data, and an absence of cross-cutting relationships between sills with possibly different ages, we do not know if emplacement (and related magmatism) occurred simultaneously (i.e., towards the end of the Cretaceous) or incrementally (i.e., between the late Aptian and the end of the Cretaceous) (e.g. Trude et al., 2003; Magee et al., 2021).

Please cite as https://doi.org/10.1016/j.jsames.2023.104314

Volcanoes, lava flows, and hydrothermal vents develop at the surface and therefore allow a better constraint on the age of magmatic activity. More specifically, the basal reflection of volcanoes and lava flows represents and thus defines the syn-volcanism paleosurface. We mapped 15 volcanoes that define two magmatic events, based on their occurrence at two discrete stratigraphic positions. The oldest volcanoes occur between the top Albian and top Cretaceous horizons, creating a high relief in the top Cretaceous paleosurface (Figure 10d). The younger volcanoes are between the Paleocene and upper Eocene strata; their basal reflection corresponds to the top Cretaceous horizon (Figure 10a-c). Associated with these younger volcanoes is a lava field that covers c. 310 km², and which was erupted onto the top Cretaceous horizon (e.g. Figure 7). We also identified four vent-like structures that can correspond to hydrothermal vents, given they have a similar geometry to the ones interpreted by Alvarenga et al. (2016) in the southwest Campos Basin. There are three Paleogene (e.g. Figure 12) and one Upper Cretaceous vent-like structures. The occurrence of volcanoes, lava flows, and hydrothermal vents at various stratigraphic levels indicates that igneous activity was episodic.

Previous works describe three main magmatic events after rift initiation in Campos Basin: late Aptian (c. 112 – 118 Ma), Santonian-Campanian (c. 70 – 80 Ma) and Paleocene – Eocene (c. 40 – 60 Ma) (Oreiro, 2006; Moreira et al., 2006; Winter et al., 2007; Thomaz Filho et al., 2008; Ren et al., 2019). Late Aptian magmatism is associated with the final breakup between the South American and African continents (Thomaz Filho et al., 2008). The two post-salt magmatic events occurred during the westward displacement of the South American plate, although its precise origin is still debated. Thomaz Filho et al. (2008) suggests these magmatic events are related to asthenospheric hot spots, a hypothesis not supported by geochemical, isotopic and paleomagnetic data (Peate, 1997; Ernesto et al., 2002; Marques and Ernesto, 2004). Oreiro et al. (2008) associate post-salt magmatism with partial melting of portions of the asthenosphere by pressure release caused by the reactivation of deep fault zones. In our study area, we note there is a greater number of sills and volcanoes to SW of the 3D volume, where

there is greater density of sub-salt faults, meaning subsalt faults might have played a role in facilitating magma transport. However, there are sills where sub-salt faults are lacking (Figure 4a, d).

Considering the interpreted igneous products in our study area, the oldest igneous event (late Aptian) could have generated the intra-salt sills. The subsequent Santonian-Campanian event resulted in eruption of the volcanoes (at two stratigraphic levels), the lava field, one hydrothermal vent, and some of the sills. The youngest event (lower Paleogene) generated three hydrothermal vents and possibly a portion of the sills.

5.2. *Salt-magma interaction*

Here we discuss (i) how salt composition and distribution affects magmatic emplacement; and (ii) the relationship between the igneous products and salt tectonics. The eight boreholes in the proximal portion of the study area show that the Aptian interval is defined by thin layers of anhydrite (e.g. Figure 11), although halite and minor amounts of more complex salts (carnallite and sylvite) become more common in the intermediate to distal parts of the basin due to remobilization during seaward salt flow (e.g. Rangel et al., 1994; Karner and Gamboa, 2007; Winter et al., 2007). Anhydrite and halite present relatively high melting temperatures and thermal conductivities, and thus rather than behaving like a fluid they can fracture during rapid magma intrusion, allowing dike emplacement (Schofield et al., 2014).

Intra-salt sills are found in different salt structures: extensional/collapsed diapirs (e.g. Figure 6), salt rollers (Figure 7), diapirs and salt anticlines (Figure 9d). Supra-salt sills occur mostly where salt is thinner, 0 – 550 ms (TWT), in the extensional domain of salt tectonics (Figure 9d,g). Supra-salt sills occur mainly in the SW of the 3D volume, and, unlike the intra-salt sills, they are interconnected forming sill-complexes (Figure 8b). The distribution of intra-

Please cite as https://doi.org/10.1016/j.jsames.2023.104314

and supra-salt sills (Figures 8b and 9d) show they do not spatially overlap, meaning the former rarely fed the latter. We therefore speculate that supra-salt sills were fed by vertical dykes, which are not imaged by our seismic reflection data (because their likely sub-vertical attitude commonly inhibits their imaging; e.g. Magee and Jackson, 2020), indicating conditions locally favoured magma ascent through the salt.

Salt tectonics in Campos Basin initiated between the late Aptian and early Albian. Previous works show the main phase of salt movement in the basin occurred from the Albian to the Maastrichtian (Demercian et al., 1993; Davison et al., 2012; Quirk et al., 2012; Amarante et al., 2021). According to these works, during the Santonian-Campanian magmatic event, the major seaward translation of salt was ongoing, forming salt and overburden structures in response to extensional and contractional deformation (Figure 1b).

Igneous intrusions occur mainly on and adjacent to the External High, where salt tectonics is characterized by extensional structures, which are associated with normal faults (Figures 9d,g). Salt and overburden structures on the External High are best-developed (i.e. are more numerous and thicker) to the SW compared to the NW, and this can be related to one or both of the following. First, this difference might simply reflect the fact that the base-salt surface is more rugose in the south (Figure 6) than the north (Figure 7), meaning the rate and style of seaward flow of salt and its overburden was more complex, resulting in formation of relatively large and abundant structures (Dooley et al., 2017; Pichel et al., 2020; Amarante et al., 2021; Erdi and Jackson 2021).

An alternative interpretation is that this along-strike change in structural style reflects varying degrees and types of salt-magma interaction. Some authors suggest that the igneous intrusions influence salt structure initiation and growth, given the elevated heat of the intrusions can enhance salt melting and movement (e.g. Magee et al., 2021; Schofield et al., 2014). However, once crystallized, the intrusions create a rigid framework that restricts salt flow and

limits the further growth of salt structures (Schofield et al., 2014; Magee et al., 2021). In this case, salt and overburden structures would continue developing where intrusions are absent. Considering these concepts and related predictions in the context of our study area, we note that a spatial relationship between salt structures and intrusions only occurs in the southern area of the 3D volume (Figure 4d). Here, sills occur where salt is welded or thin (up to 100 ms TWT), or bordering salt structures. In this southern area, there is an overall greater density of supra-salt sills (Figure 8b). This may indicate that a great density of supra-salt sills can impact the development of salt structures, locally restricting salt rise by creating a rigid framework in the overburden (following Magee et al., 2021; Schofield et al., 2014). Put another way, large salt structures could only develop where supra-salt sills were absent. However, we argue that magmatic emplacement did not influence the overall style and distribution of thin-skinned salt-related deformation, which was instead controlled by margin-wide gravity gliding above prominent base-salt relief (Amarante et al., 2021).

Another possible interpretation, proposed by Fiduk et al. (2004), is that pre-existing salt structures, formed by some other means (e.g., reactive diapirism during thin-skinned extension), can control the spatial distribution of igneous intrusions, given that intruding magma can ascend through salt and use associated faults as high permeability pathways through the overlying and adjacent sedimentary section. In this case, sills would preferentially be located on or adjacent to salt structures that are associated with overburden faulting, with feeder dikes present within the salt. Although sills in the study area are often located adjacent to salt structures, the relationship between sills and salt-related faulting is unclear. Sometimes sills develop within normal faults (Figure 9a,d; Figure 6 sills 3 – 6, Figure 10a,a1), indicating they utilized the faults as pathways. However, there are numerous examples where sills are not spatially related to salt-related faulting (Figure 9b,c Figure 5 sills 9 – 10, Figure 6 sill 9, Figure 10d). Therefore, salt tectonics possibly partially influenced the distribution of intrusions. Extrusive igneous products (volcanoes and lava flows) developed mostly after the main phase

of salt movement (i.e., Albian – Maastrichtian), and we observe a spatial relationship between volcanoes and lava fields, and salt-tectonic structures. For example, volcanoes developed above areas where salt was welded or very thin (up to 100 ms TWT) (Figure 4d), meaning that the volcanoes were dyke-fed and it was easier for the dykes to get through the salt where it was thin. Lava fields were fed by the eruptions, and so their distribution and thickness were dependent of the relief of the top Cretaceous surface, which was itself controlled by salt movement (Figure 4e), i.e. lava fields are typically thicker in the paleolows and thinner to absent in paleohighs (Figures 7 and 4e).

6. Conclusions

We used 2D and 3D seismic reflection and borehole data from the southern Campos Basin to map and characterize post-salt igneous sills and volcanoes, and understand the interaction between salt tectonics and igneous products. The key conclusions of our study are:

- The southern Campos Basin contains intrusive and extrusive igneous products. We mapped 99 sills emplaced within uppermost Aptian-to-Maastrichtian strata, 83 emplaced above the salt and 16 intra-salt, and 15 volcanoes within Upper Cretaceous-to-lower Paleogene strata, associated with a >310 km² lava field. We also identified four vent-like structures at two stratigraphic levels, sub-salt to Paleogene and sub-salt to Upper Cretaceous.
- The occurrence of volcanoes, lava flows, and hydrothermal vents at various stratigraphic levels indicates that Cretaceous-to-Paleogene igneous activity was punctuated, rather than synchronous.
- The spatial and genetic relationship between igneous intrusions and salt tectonics is complex. Sills emplacement locally influenced salt tectonics. In the

Please cite as https://doi.org/10.1016/j.jsames.2023.104314

southern portion of the 3D seismic volume, numerous sill complexes are present, with intrusions possibly restricting salt movement by creating a rigid framework in the overburden, limiting the growth of large salt structures. However, the intrusions do not affect the overall style of regional, thin-skinned deformation, which was controlled by margin-wide gravity gliding across prominent base-salt relief.

- Salt structures and related faulting partially influenced the distribution and location of intrusions emplacement by acting as pathways to intruding magma.
- The relationship between extrusive igneous products and salt tectonics is more straightforward. Salt distribution influenced the location of volcanoes, giving they developed where salt is welded of very thin; lava field distribution and thickness were controlled by the paleorelief originated by salt tectonics, with flows ponding in paleolows generated by salt withdrawal.

Acknowledgments

F.B.d. Amarante thanks CNPq (National Council for Scientific and Technological Development of Brazil) for the doctorate scholarships. We thank Craig Magee and the two anonymous reviewers for their constructive insights, and the editor-in-chief Andres Folguera for his editorial handling. The authors gratefully acknowledge ANP (Brazil's National Oil, Natural Gas and Biofuels Agency) for providing the data and for the license to publish this article.

References

Almeida, F.F.M., 2006. Ilhas oceânicas brasileiras e suas relações com a tectônica atlântica. Terræ Didatica 2(1), 3–18.

Alvarenga, R.S., Iacopini, D., Kuchle, J., Scherer, C.M.S., Goldberg, K., 2016. Seismic characteristics and distribution of hydrothermal vent complexes in the Cretaceous offshore rift section of the Campos Basin, offshore Brazil., Marine and Petroleum Geology 74, 12–25. https://doi.org/10.1016/j.marpetgeo.2016.03.030

Amarante, F.B., Jackson, C.A., Pichel, L.M., Scherer, C.M.S., Kuchle, J., 2021. Pre-salt rift morphology controls salt tectonics in the Campos Basin, offshore SE Brazil. Basin Research 33 (5), 2837–2861. https://doi.org/10.1111/bre.12588

Aslanian, D., Moulin, M., Olivet, J.-L., Unternehr, P., Matias, L., Bache, F., Rabineau, M., Nouzé, H., Klingelhoefer, F., Contrucci, I., Labails, C., 2009. Brazilian and African passive margins of the central segment of the South Atlantic Ocean: kinematic constraints. Tectonophysics 468, 98–112.

Baksi, A.K., 2018. Paraná flood basalt volcanism primarily limited to ~ 1 Myr beginning at 135 Ma: New 40 Ar/ 39 Ar ages for rocks from Rio Grande do Sul, and critical evaluation of published radiometric data. Journal of Volcanology and Geothermal Research 355, 66–77. https://doi.org/10.1016/j.jvolgeores.2017.02.016

Chang, H.K., Kowsmann, R.O., Figueiredo, A.M.F., Bender, A., 1992. Tectonics and stratigraphy of the East Brazil rift system: an overview. Tectonophysics 213, 97–138.

Cobbold, P.R., Szatmari, P., 1991. Radial gravitational gliding on passive margins. Tectonophysics 188, 249–289. https://doi.org/10.1016/0040-1951(91)90459-6

Cohen, K.M., Finney, S.C., Gibbard, P.L., Fan, J.-X., 2013; updated. The ICS International Chronostratigraphic Chart. Episodes 36, 199–204.

Contrucci, I., Matias, L., Moulin, M., Geli, L., Klingelhofer, F., Nouze, H., Aslanian, D., Olivet, J.-L., Rehault, J.-P., Sibuet, J.-C., 2004. Deep structure of the West African continental margin (Congo, Zaïre, Angola), between 5°S and 8°S, from reflection/refraction seismics and gravity data. Geophysical Journal International 158, 529–553.

Contreras, J., Zühlke, R., Bowman, S., Bechstadt, Th, 2010. Seismic stratigraphy and subsidence analysis of the southern Brazilian margin (Campos, Santos and Pelotas basins). Marine and Petroleum Geology 27, 1952–1980.

Correia, U.M. da C., Honório, B.C.Z., Kuroda, M.C., Melani, L.H., Vidal, A.C., 2019. Geometric characterization of igneous intrusions: 3-D seismic insights from the Campos Basin, SE Brazil., Marine and Petroleum Geology 102, 725–739. https://doi.org/10.1016/j.marpetgeo.2019.01.022

Demercian, S., Szatmari, P., Cobbold, P.R., 1993. Style and pattern of salt diapirs due to thin-skinned gravitational gliding, Campos and Santos basins, offshore Brazil. Tectonophysics 228 (3–4), 393–433.

Davison, I., Anderson, L., Nuttall, P., 2012. Salt deposition, loading and gravity drainage in the Campos and Santos salt basins. Geological Society, London, Special Publications 363, 159–174. https://doi.org/10.1144/sp363.8

Dooley, T.P., Hudec, M.R., Carruthers, D., Jackson, M.P.A., Luo, G., 2017. The effects of base-salt relief on salt flow and suprasalt deformation patterns — Part 1: Flow across simple steps in the base of salt. Interpretation 5, SD1–SD23. https://doi.org/10.1190/int-2016-0087.1

Eide, C.H., Schofield, N., Lecomte, I., Buckley, S.J., Howell, J.A. 2018. Seismic interpretation of sill-complexes in sedimentary basins: The 'sub-sill imaging problem'. Journal of the Geological Society 175, 193–209.

Ernesto, M., Marques, L. S., Piccirillo, E. M., Molina, E. C., Ussami, N., Comin-Chiaramonti, P., Bellieni, G. (2002). Paraná Magmatic Province-Tristan da Cunha plume system: fixed versus mobile plume, petrogenic considerations and alternative heat sources. Journal of Volcanology and Geothermal Research 118, 15–36.

Evain, M., Afilhado, A., Rigoti, C., Loureiro, A., Alves, D., Klingelhoefer, F., Schnurle, P., Feld, A., Soares, J., Vinicius de Lima, V., Corela, C., Matias, L., Benabdellouahed, M., Baltzer, A., Rabineau, M., Viana, A., Moulin, M., Aslanian, D., 2015. Deep structure of the Santos Basin-São Paulo plateau system, SE Brazil. Geophys. Res. Solid Earth 120. https://doi.org/10.1002/2014JB011561

Fiduk, J.C., Brush, E.R., Anderson, L.E., Gibbs, P.B., Rowan, M.G., 2004. Salt Deformation, Magmatism, and Hydrocarbon Prospectivity in the Espirito Santo Basin, Offshore Brazil. 24th Annual Bob F. Perkins Research Conference, GCSSEPM, Houston, Texas. https://doi.org/10.5724/gcs.04.24.0640

Fiduk, J.C., Rowan, M.G., 2012. Analysis of folding and deformation within layered evaporites in Blocks BM-S-8 & -9, Santos Basin, Brazil. Geological Society, London, Special Publications 363, 471–487. https://doi.org/10.1144/sp363.22

Guardado, L.R., Gamboa, L.A.P., Lucchesi, C.F., 1989. Petroleum geology of Campos Basin, Brazil: a model for producing Atlantic type basin. In: Edwards, J.D., Santagrossi, P.A. (Eds.), Divergent/Passive Margins Basins. AAPG Memoir 48, 3–36.

Guardado, L.R., Spadini, A.R., Brandão, J.S.L., Mello, M.R., 2000. Petroleum system of the Campos Basin, Brazil. In: Mello, M.R., Katz, B.J. (Eds.), Petroleum Systems of South Atlantic Margins. AAPG Memoir 73, 317–324.

Heilbron, M., Mohriak, W.U., Valeriano, C.M., Milani, E.J., Almeida, J., Tupinambá, M., 2000. From collision to extension: The roots of the southeastern continental margin of Brazil, in: Atlantic Rifts and Continental Margins. American Geophysical Union, pp. 1–32. https://doi.org/10.1029/gm115p0001

Heimdal, T.H., Callegaro, S., Svensen, H.H., Jones, M.T., Pereira, E., Planke, S., 2019. Evidence for magma–evaporite interactions during the emplacement of the Central Atlantic Magmatic Province (CAMP) in Brazil. Earth and Planetary Science Letters 506, 476–492. https://doi.org/10.1016/j.epsl.2018.11.018

Li, C., Ripley, E.M., Naldrett, A.J., Schmitt, A.K., Moore, C.H., 2009. Magmatic anhydrite-sulfide assemblages in the plumbing system of the Siberian Traps. Geology, 37(3), 259–262. https://doi.org/10.1130/G2535 5A.1

López-García, J.M., Moreira, D., Benzerara, K., Grunewald, O., López-García, P., 2020. Origin and evolution of the halo-volcanic complex of Dallol: Proto-volcanism in Northern Afar (Ethiopia). Frontiers in Earth Science, 7, 351. https://doi.org/10.3389/feart.2019.00351

Magee, C., Jackson, C.-L., 2020. Seismic reflection data reveal the 3D structure of the newly discovered Exmouth Dyke Swarm, offshore NW Australia. Solid Earth, 11 (2), 576–606.

Magee, C., Pichel, L.M., Madden-Nadeau, A.L., Jackson, C.A. -L., Mohriak, W., 2021. Salt–magma interactions influence intrusion distribution and salt tectonics in the Santos Basin, offshore Brazil., Basin Research 33, 1820–1843. https://doi.org/10.1111/bre.12537

Mark, N.J., Schofield, N., Pugliese, S., Watson, D., Holford, S., Muirhead, D., Brown, R., Healy, D., 2018. Igneous intrusions in the Faroe Shetland basin and their implications for hydrocarbon exploration; new insights from well and seismic data. Marine and Petroleum Geology 92, 733–753. https://doi.org/10.1016/j.marpetgeo.2017.12.005

Marques, L. S., Ernesto, M., 2004. O magmatismo toleítico da Bacia do Paraná. In: V. M. Neto, A. Bartorelli, C. D. Carneiro, B. B. de Brito-Neves (Eds.), Geologia do continente Sul-Americano: evolução da obra de Fernando Flávio Marques de Almeida. São Paulo: Beca, 245–263.

Mohriak, W.U., Mello, M.R., Karner, G.D., Dewey, J.F., Maxwell, J.R., 1989. Structural and stratigraphic evolution of the Campos Basin, offshore Brazil. In: Tankard, A.J., Balkwill, H.R. (Eds.), Extensional Tectonics and Stratigraphy of the North Atlantic Margins. AAPG Memoir 46, 577–598.

Mohriak, W.U., Nemcok, M., Enciso, G., 2008. South Atlantic divergent margin evolution: rift-borded uplift and salt tectonics in the basins of Southeastern Brazil. In: Pankhurst, R.J., Trouw, R.A.J., Brito Neves, B.B., de Wit, M.J. (Eds.), West Gondwana Pre-Cenozoic Correlations across the South Atlantic Region, vol. 294. Geological Society of London, Special Publications, 365–398.

Mohriak, W., 2020. Genesis and evolution of the South Atlantic volcanic islands offshore Brazil. Geo-Marine Letters 40, 1–33. https://doi.org/10.1007/s00367-019-00631-w

Mohriak, W.U., Gordon, A., Mello, M.R., 2021. Chapter 11: Origin and Petroleum System of the Cabo Frio High Between the Santos and Campos Basins: Reviewed Integration of Structural and Paleogeographic Reconstruction with the Oil and Gas Systems. AAPG Memoir 124, 273–324. https://doi.org/10.1306/13722323msb.11.1853

Moreira, J.L., Esteves, C.A., Rodrigues, J.J.G., Vasconcelos, C.S., 2006. Magmatismo, sedimentação e estratigrafia da porção norte da Bacia de Santos. Boletim de Geociências da Petrobras 14 (1), 161–170.

Oreiro, S.G., 2006. Magmatismo e sedimentação em uma área na Plataforma Continental de Cabo Frio, Rio de Janeiro, Brasil, no intervalo Cretáceo Superior – Terciário. Boletim de Geociências da Petrobras 14 (1), 95–112.

Oreiro, S.G., Cupertino, J.A., Szatmari, P., Thomaz Filho, A., 2008. Influence of pre-salt alignments in post-Aptian magmatism in the Cabo Frio High and its surroundings, Santos and Campos basins, SE Brazil: An example of non-plume-related magmatism. Journal of South American Earth Sciences 25, 116–131.

Peate, D., 1997. The Paraná-Etendeka province. In: J. J. Mahoney, M. F. Coffin (Eds.), Large igneous provinces: continental, oceanic, and planetary flood Volcanism. American Geophysical Union, Washington D.C., 217–245.

Planke, S., Rasmussen, T., Rey, S.S., Myklebust, R., 2005. Seismic characteristics and distribution of volcanic intrusions and hydrothermal vent complexes in the Vøring and Møre basins. In: Dore, A.G., Vining, B.A. (Eds.), North-west Europe and Global Perspectives: Proceedings of the Sixth Petroleum Geology Conference, vol. 6. Geological Society of London, 833–844. https://doi.org/10.1144/006083

Planke, S., Symonds, P.A., Alvestad, E., Skogseid, J., 2000. Seismic volcanostratigraphy of large-volume basaltic extrusive complexes on rifted margins. Journal of Geophysical Research: Solid Earth 105 (B8), 19335–19351. https://dx.doi.org/10.1029/1999JB900005

Quirk, D.G., Schødt, N., Lassen, B., Ings, S.J., Hsu, D., Hirsch, K.K., Von Nicolai, C., 2012. Salt tectonics on passive margins: examples from Santos, Campos and Kwanza basins. Geological Society, London, Special Publications 363, 207–244. https://doi.org/10.1144/sp363.10

Rangel, H.D., Martins, F.A.L., Esteves, F.R., Feijó, F.J., 1994. Bacia de Campos. Boletim de Geociências da Petrobras 8 (1), 203–218.

Ren, K., Oliveira, M.J.R., Zhao, J., Zhao, J., Oliveira, L.C., Rancan, C.C., Carmo, I.O., Deng, Q., 2019. Using Wireline Logging and Thin Sections to Identify Igneous Contact Metamorphism and Hydrothermal Influence on Presalt Limestone Reservoirs in Libra Block, Santos Basin. Offshore Technology Conference, Rio de Janeiro, Brazil, 29–31 October 2019, v. OTC-29818-MS, p. 10.

Thomaz Filho, A., Mizusaki, A.M.P., Antonioli, L., 2008. Magmatismo nas bacias sedimentares brasileiras e sua influência na geologia do petróleo. Revista Brasileira de Geociências 38 (2),128–137.

Trude, J., Cartwright, J., Davies, R.J., Smallwood, J.R., 2003. New technique for dating igneous sills. Geology 31, 4. https://doi.org/10.1130/G19559.1

Schofield, N., Alsop, I., Warren, J., Underhill, J.R., Lehné, R., Beer, W., Lukas, V., 2014. Mobilizing salt: Magma-salt interactions. Geology, 42 (7), 599–602. https://doi.org/10.1130/G35406.1

Szatmari, P., 2000. Habitat of petroleum along the South Atlantic margins. In: Mello, M.R., Katz, B.J. (Eds.), Petroleum Systems of South Atlantic Margins: AAPG Memoir 73, 69–75.

Winter, W.R., Jahnert, R.J., França, A.B., 2007. Bacia de Campos. Boletim de Geociências da Petrobras 15(2), 511–529.

Zalán, P.V., Severino, M.C.G., Oliveira, J.A.B., Magnavita, L.P., Mohriak, W.U., Gontijo, R.C., Viana, A.R., Szatmari, P., 2009. Stretching and thinning of the upper lithosphere and continental-oceanic crustal transition in southeastern Brazil. November. In: AAPG International Conference & Exhibition Abstracts Volume CD-ROM, Paper 653274, Rio de Janeiro, Brazil, pp. 15–18.